ELSEVIER

Journal of Alloys and Compounds 323–324 (2001) 534–539

Journal of ALLOYS AND COMPOUNDS

www.elsevier.com/locate/jallcom

Rare earth ion conduction in solids

G. Adachi*, N. Imanaka, S. Tamura

Department of Applied Chemistry, Faculty of Engineering, Osaka University, 2-1 Yamadaoka, Suita, Osaka 565-0871, Japan

Abstract

The trivalent cation conductors of $R_2(MO_4)_3$ (R: Al, Sc, Y, Er–Lu; M: W, Mo) polycrystals in the tungstate and the molybdate series were prepared and the trivalent R^{3+} conducting properties were investigated. The ion conductivity was found to be strongly dependent on the crystal lattice size and the highest conductivity was obtained in $Sc_2(WO_4)_3$ and $Sc_2(MoO_4)_3$, respectively, among each series. In addition, the relationship between the lattice size and R^{3+} ion conduction was also clarified by making various types of solid solutions and the enhancement of the objective R^{3+} ion conduction was successfully realized. The conducting species in these solid electrolytes was directly demonstrated to be trivalent Sc^{3+} cation by a dc electrolysis.

Keywords: Rare earths; $Sc_2(WO_4)_3$ type; Trivalent ion; Solid electrolytes

1. Introduction

Various types of solid electrolytes have been eagerly investigated so far. The majority of the solid electrolytes are monovalent and divalent cationic conductors and oxide anionic conductors, showing a high ionic conductivity, and some of them have been already put on the market, e.g. oxygen gas sensors based on yttria stabilized zirconia and lithium batteries for heart pacemaker. In contrast, the trivalent cation had generally been believed not to migrate in solids due to the strong electrostatic interaction between the trivalent cation and the surrounding constituent ions of the structure such as O^{2-}. Some papers had claimed that Ln^{3+}-β″-alumina [1–7], β-$LaNbO_3$ [8] and $LaAl_{11}O_{18}$ [9] are the trivalent ion conductors. However, these papers have neither directly nor quantitatively demonstrated any trivalent ion migration in solids. Among them, especially Ln^{3+}-β″-alumina solid electrolytes were prepared by ionically exchanging Na^+ site in Na^+-β″-alumina for Ln^{3+}. Therefore, small amount of sodium ion still remains in these solid electrolytes and might contribute for ion conduction. For realizing a trivalent cation conduction in solids, it is necessary to reduce strong interaction between the mobile trivalent cations and the lattice conforming anions. Recently, $R_2(MO_4)_3$ (R: Al, In, Sc, Y, Er–Lu; M: W, Mo) solid electrolytes with the orthorhombic $Sc_2(WO_4)_3$ type structure which is illustrated in Fig. 1, were demonstrated to show the trivalent R^{3+} cation conduction [10–16]. The tungstates with larger rare earths in the lanthanoid series, have another structure of $Eu_2(WO_4)_3$ type with monoclinic symmetry (Fig. 1), and those tungstates are insulating. The $Sc_2(WO_4)_3$ type structure is a quasi-layered and has a large pathway where R^{3+} ion can migrate smoothly as shown in Fig. 2. In this structure, hexavalent tungsten ion bonds to surrounding four oxide anions to form a WO_4^{2-} tetrahedron unit, resulting in the considerable reduction of the electrostatic interaction between R^{3+} and O^{2-} and the realization of the R^{3+} ion conduction.

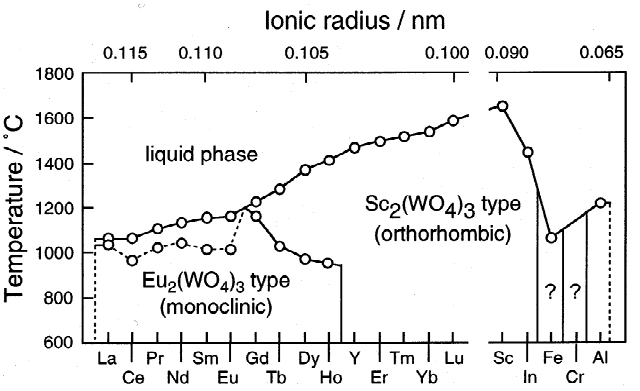

Fig. 1. The structure type of the $R_2(WO_4)_3$ tungstates.

*Corresponding author. Tel.: +81-6-6879-7352; fax: +81-6-6879-7354.

E-mail address: adachi@chem.eng.osaka-u.ac.jp (G. Adachi).

0925-8388/01/$ – see front matter
PII: S0925-8388(01)01138-0

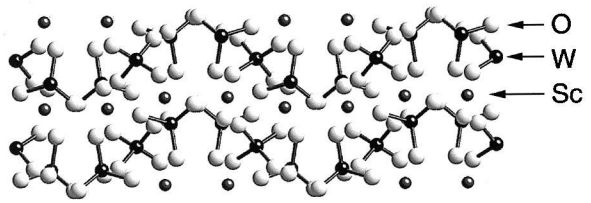

Fig. 2. The $Sc_2(WO_4)_3$ type structure in *b*-axis direction.

Table 1 tabulates the various demonstration methods of trivalent ionic conduction for solid electrolytes claimed as trivalent cation conductors. The methods utilized for Ln^{3+}-β″-alumina, β-$LaNbO_3$ and $LaAl_{11}O_{18}$ are limited to only some methods and the demonstration is still indirect and not quantitative. In contrast, the electrical properties of the $Sc_2(WO_4)_3$ type solid electrolytes are investigated by all the methods listed in the table, especially the dc electrolysis was successfully completed which can definitely identify the mobile species.

In this paper, we investigate the rare earth ion conducting properties in $R_2(MO_4)_3$ polycrystalline single phase and some solid solutions with the $Sc_2(WO_4)_3$ type polycrystals, and describe the direct demonstration of the R^{3+} trivalent ion conduction in solids.

2. Experimental

2.1. Sample preparation

$R_2(MO_4)_3$ (R: Sc, Y, Er–Lu; M: W, Mo) was prepared by a conventional solid state reaction using high purity R_2O_3(99.9%) and MO_3(99.9%) as the starting materials. After pulverized in a mortar and pelletized, the pellets were calcined at 1000°C for 12 h successively until the sample color became white (light pink for $Er_2(MO_4)_3$) in air atmosphere. The sample pellets were finally sintered at 1050–1200°C for 12 h. $Al_2(MO_4)_3$ was synthesized from $Al(OH)_3$(99.9%) and MO_3. After the powder was mixed in a mortar, the calcination procedure was repeated at 1000°C for 12 h until the sample color became white and the sintering was carried out at 1100°C for 12 h in air atmosphere.

$Sc_2(WO_4)_3$–$Gd_2(WO_4)_3$ solid solutions were prepared from reagent grade of Sc_2O_3, Gd_2O_3(99.9%), and WO_3. A stoichiometric amount of them was mixed, and heated at 1000°C for 12 h and then 1200°C for 12 h. Obtained powder was pelletized and sintered at 1200°C for 12 h. $Al_2(WO_4)_3$–$Sc_2(WO_4)_3$-$Lu_2(WO_4)_3$ solid solutions were prepared by mixing $Al_2(WO_4)_3$ and $Sc_2(WO_4)_3$–$Lu_2(WO_4)_3$ solid solution. At first, $Sc_2(WO_4)_3$–$Lu_2(WO_4)_3$ solid solutions were prepared by mixing an appropriate amount of Sc_2O_3, Lu_2O_3, and WO_3 and heating at 1000°C for 12 h and then at 1200°C for 12 h. $Al_2(WO_4)_3$ prepared was mixed with the $Sc_2(WO_4)_3$–$Lu_2(WO_4)_3$ solid solution and heated at 1000°C for 12 h in air atmosphere. The sintering procedure was carried out at 1200°C for 12 h in air.

All samples prepared were identified by X-ray powder diffraction (XRD) using Cu Kα radiation (M18XHF, Mac Science). The XRD data were collected by a step-scanning method in the 2θ range from 10° to 70° with a step width of 0.04° and a scan time of 4 s. The XRD patterns obtained were analyzed using the Rietveld refinement program RIETAN-94 [17].

2.2. Measurements

The surface of all polycrystalline samples was polished and Pt sputtered layer (diameter: 0.62 cm) was formed on both center surfaces of the sample pellet as the electrode. In the case of the measurements at temperatures over 600°C, the Pt paste was utilized in spite of the Pt sputtered layer. An ac conductivity was measured by using a LCR meter (8284A, Hewlett-Packerd) at the frequency range from 20 Hz to 1 MHz in the temperature range between 300 and 800°C. Oxygen partial pressure dependencies of the ac conductivity was investigated in O_2, He, N_2, air, and CO–CO_2 mixed gas. A dc conductivity was measured in the different oxygen partial pressure atmosphere by monitoring the voltage generated between two Pt electrodes when the constant dc current of 0.1 μA was passed through the sample pellet at 700°C. The dc electrolyses were performed by applying the dc voltage of 1–3 V between two Pt blocking electrodes sandwiching the sample for 200–400 h.

Table 1
Comparison of the experimental methods which have been applied (○) or not (–), to characterize the compounds for which a multivalent cationic conduction is assumed[a]

Ionic conducting compound	Impedance spectroscopy	Polarization measurements	Conductivity or polarization in different atmosphere	EMF measurements	dc electrolysis + detailed analysis
M^{3+}-β″-alumina (IE)	○	–	–	–	–
β-Alumina related phases	○	–	–	○	–
β-$LaNb_3O_9$	○	○	○	○	–
$Sc_2(WO_4)_3$ type phases	○	○	○	○	○

[a] β-Alumina compounds which are prepared by ion-exchange are denoted by (IE).

3. Results and discussion

3.1. $R_2(MO_4)_3$ polycrystals

The tungstates and molybdates, $R_2(MO_4)_3$, including Y and heavy rare earths, Er–Lu, as R^{3+} cation, were appreciably hygroscopic at room temperature and the dehydration was observed at around 120°C from TG–DTA measurements. Therefore, the XRD analyses were carried out after heating at 150°C in vacuum. All $R_2(MO_4)_3$ were found to possess the single phase of $Sc_2(WO_4)_3$ type structure which is assigned to orthorhombic symmetry (space group *Pbcn*) and the XRD patterns of the sample were shifted toward a lower degree in 2θ with increasing trivalent ionic radius in the tungstates and molybdates. The unit cell volume monotonously enhanced with increasing the trivalent cationic radius in both systems.

Fig. 3 shows the trivalent cation radius dependencies of the electrical conductivity at 600°C and the activation energy for $R_2(WO_4)_3$ and $R_2(MoO_4)_3$. In both systems, the solid electrolyte containing Sc^{3+} as the trivalent cation shows the highest conductivity and the lowest activation energy, which indicates that Sc^{3+} is the most suitable trivalent cation for the conduction in both solid electrolyte series with the $Sc_2(WO_4)_3$ type structure. In the case of the larger trivalent cations than the suitable trivalent ion of Sc^{3+}, the electrical conductivity decreased and the activation energy increased with the R^{3+} radius increase since the R^{3+} ion size to the lattice size ratio increases and, as a result, the electrostatic interaction with surrounding oxide anions becomes stronger. On the other hand, for the smaller ion such as Al^{3+}, the conductivity reduced and activation energy increased compared with the case for the Sc^{3+} ion migration. This might be ascribed to the high electrostatic interaction caused by its low polarizability.

Since the oxide or the hydroxide with the cation whose valency is higher than divalent state were used as the starting materials, the candidate conducting species were limited to the cation species of R^{3+} or M^{6+}, O^{2-}, electron, or hole in the $R_2(MO_4)_3$ solid electrolytes. In order to clarify the conducting characteristics in $R_2(MO_4)_3$, the ac and the dc conductivity were measured in different oxygen pressure atmospheres.

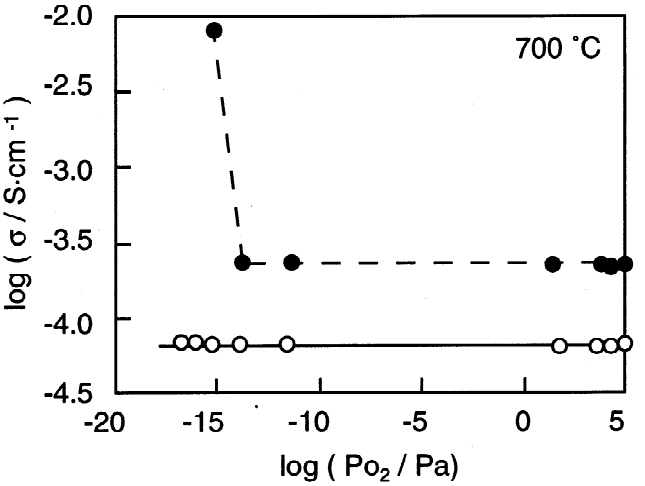

Fig. 4. Oxygen partial pressure dependencies of the ac conductivity for $R_2(WO_4)_3$ (○) and $R_2(MoO_4)_3$ (●) at 700°C.

Fig. 4 presents the oxygen partial pressure dependencies of the ac conductivity at 700°C for $Sc_2(WO_4)_3$ and $Sc_2(MoO_4)_3$ which possess the highest conductivity among the tungstates and the molybdates. The conductivity of both $Sc_2(WO_4)_3$ and $Sc_2(MoO_4)_3$ maintained a constant value in the wide oxygen pressure range($Sc_2(WO_4)_3$: 10^{-17}–10^{5} Pa, $Sc_2(MoO_4)_3$: 10^{-13}–10^{5} Pa), indicating that predominant conducting species is ion in the above mentioned oxygen pressure region. However, the ac conductivity of $Sc_2(MoO_4)_3$ drastically increased at the oxygen pressures lower than 10^{-13} Pa. The increase of the ac conductivity in low O_2 pressure region means that the n-type electronic conduction which might be caused by the reduction of Mo^{6+} in a reducing atmosphere appears.

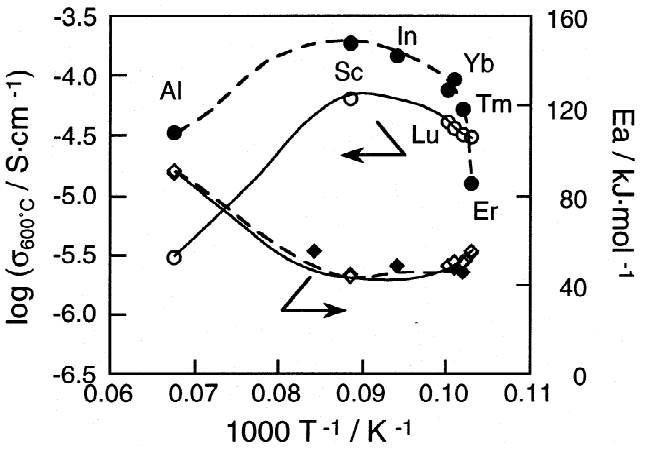

Fig. 3. The R^{3+} radius dependencies of the electrical conductivity and activation energy for $R_2(WO_4)_3$ (○, ◊) and $R_2(MoO_4)_3$ (●, ♦) at 600°C.

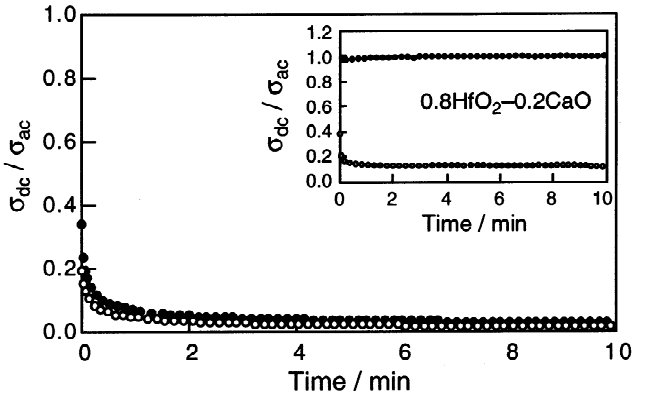

Fig. 5. The dc to ac conductivity ratio(σ_{dc}/σ_{ac}) of the $Sc_2(WO_4)_3$ in O_2(●) and He (○) atmosphere plotted as the function of time. The corresponding datum of a representative O^{2-} ion conductor of $0.8HfO_2$–0.2CaO is inserted.

Fig. 5 plots the dc to the ac conductivity ratio (σ_{dc}/σ_{ac}) for $Sc_2(WO_4)_3$ as the function of the time at 700°C. In the case of oxide anionic conductors, the polarizing behaviors between O_2 and the atmosphere in a low O_2 pressure were quite different [10] as inserted in the figure. That is, the σ_{dc}/σ_{ac} ratio is equivalent to one in O_2 atmosphere since a dc conductivity is exactly equal to an ac conductivity by successively supplying the O^{2-} ion into the solid electrolyte from O_2 gas in the atmosphere, while the σ_{dc}/σ_{ac} ratio abruptly decreases in a low O_2 pressure atmosphere such as He because the O^{2-} ion can not be introduced into the solid electrolyte. In the case of $Sc_2(WO_4)_3$, a steep polarization behavior was observed even in the O_2 atmosphere and this result indicates that the O^{2-} ion conduction in $Sc_2(WO_4)_3$ was eliminated. Furthermore, $Sc_2(MoO_4)_3$ also shows a similar polarization behavior as demonstration in Fig. 5.

From the results as described above, the conducting species in $R_2(MO_4)_3$ is further limited to the cation species of R^{3+} and M^{6+}. In order to directly identify the migrating cation species in $Sc_2(WO_4)_3$, the dc electrolysis was carried out using the Pt bulk as the blocking electrode at 700°C. By applying the dc voltage of 3 V which is higher than the decomposition voltage of ca. 2 V, the mobile cation species migrates from the anode to the cathode direction in the sample, and segregates on the cathodic surface which is in contact with the Pt bulk electrode.

Fig. 6 shows the scanning electron microscopic (SEM) photograph of the cathodic surface of the sample after the electrolysis. Many deposits were recognized at the surface and they were identified to be Sc_6WO_{12} by EPMA and micro X-ray diffraction analysis. On the other hand, the plate shape deposits identified as WO_3 from the micro X-ray diffraction analysis were observed on the anodic surface of the sample pellet. These results clearly support the idea that the Sc^{3+} migrates to the cathode direction and reacts with mother $Sc_2(WO_4)_3$ phase and forms Sc_6WO_{12} at the cathodic surface by applying the dc voltage higher than the decomposition voltage, while the WO_3 remains at the anodic surface after Sc^{3+} migration as described in the following equations.

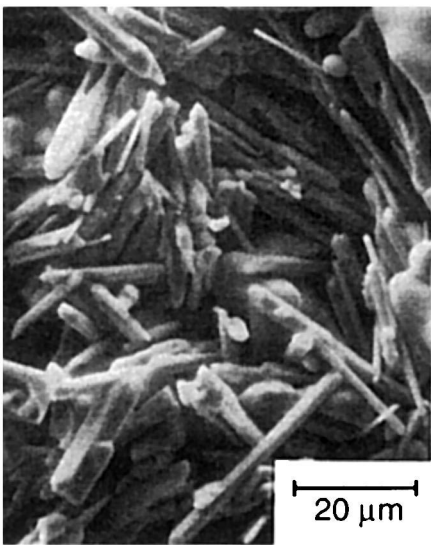

Fig. 6. The SEM photograph at the cathodic surface of the $Sc_2(WO_4)_3$ pellet after dc electrolysis.

(Anodic surface) $2Sc_2(WO_4)_3 \rightarrow 4Sc^{3+} + 6WO_3 + 3O_2 + 12e^-$

(Cathodic surface) $4Sc^{3+} + Sc_2(WO_4)_3 + 12e^- \rightarrow Sc_6WO_{12}$

The molybdates, $R_2(MoO_4)_3$, have been also demonstrated to show the trivalent R^{3+} conduction in its lattice structure by the same way mentioned above. The deposits were also observed at cathodic surface after the dc electrolysis. However, the deposits were found to contain only Sc element by EPMA. This means that the deposits are Sc_2O_3. The Sc^{3+} ion migrated to the cathodic surface is reduced to a Sc metal, and then the Sc metal immediately reacted with O_2 in the atmosphere at the operating temperature of 700°C. The anodic surface of the sample is exactly the same as the mother phase of $Sc_2(MoO_4)_3$, because MoO_3 which was left at the anodic surface after the Sc^{3+} migration, vaporized at the operation temperature of 700°C.

The conducting species in $R_2(MO_4)_3$ was directly and clearly demonstrated to be the trivalent R^{3+} cation and neither electron, hole, nor O^{2-} anion by the above mentioned researches.

3.2. Solid solutions

Among the $R_2(MO_4)_3$ solid electrolytes, the Sc^{3+} is found to be the most suitable cation among rare earth series in the $Sc_2(WO_4)_3$ type structure. For the purpose of successively investigating the detail relationship between the objective R^{3+} ion conductivity and the lattice size variation of the $Sc_2(WO_4)_3$ type solid electrolyte, we prepared the various types of solid solutions [18–20] whose lattice size was intentionally varied by changing the mixing ratio of the different size trivalent cations in the solid solution system (ionic radius; Sc^{3+}: 0.0885 nm [21], Gd^{3+}: 0.1078 nm [21]).

Fig. 7 shows the composition dependencies of the conductivity for the $(1-x)Sc_2(WO_4)_3$–$xGd_2(WO_4)_3$ system. The $(1-x)Sc_2(WO_4)_3$–$xGd_2(WO_4)_3$ solid solutions were found to possess the $Sc_2(WO_4)_3$ type structure in the range $0<x\leq 0.6$ and the $Eu_2(WO_4)_3$ type structure in the range of x higher than 0.6 by the XRD measurements. The conductivity increased up to $x=0.2$ and decreased by the further substitution. The $0.8Sc_2(WO_4)_3$–$0.2Gd_2(WO_4)_3$ showed the highest conductivity which was three times as

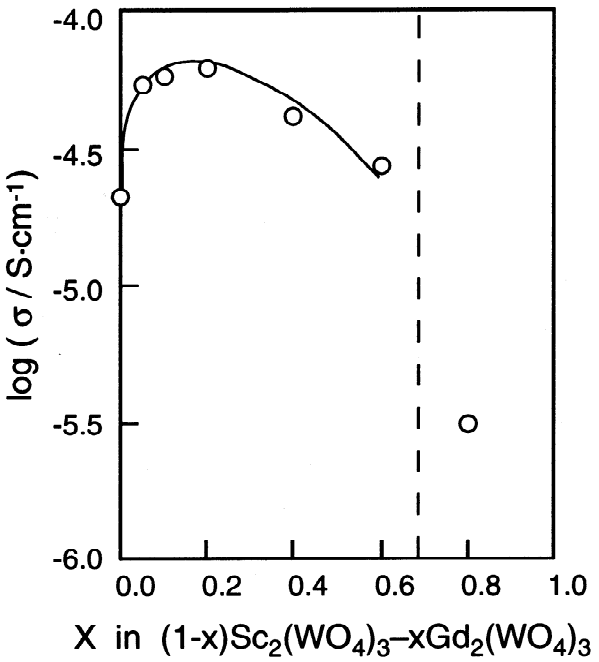

Fig. 7. The composition dependencies of the conductivity for the $(1-x)Sc_2(WO_4)_3$–$Gd_2(WO_4)_3$ solid solution at 600°C.

high as that of pure $Sc_2(WO_4)_3$. In the region of x greater than 0.6, the conductivity drastically decreased since the structure changed from $Sc_2(WO_4)_3$ type to $Eu_2(WO_4)_3$ type structure. For the purpose of investigating the possibility of the electronic conduction, the oxygen–air gas concentration cell was fabricated with $(1-x)Sc_2(WO_4)_3$–$xGd_2(WO_4)_3$ ($x=0.2$ and 0.8) and the EMF was measured at the temperature range between 600 and 900°C. The EMF values obeyed theoretically to the Nernst equation derived from the gas concentration cell in the case of $0.8Sc_2(WO_4)_3$–$0.2Gd_2(WO_4)_3$. However, the EMFs of $0.2Sc_2(WO_4)_3$–$0.8Gd_2(WO_4)_3$ were constant value of

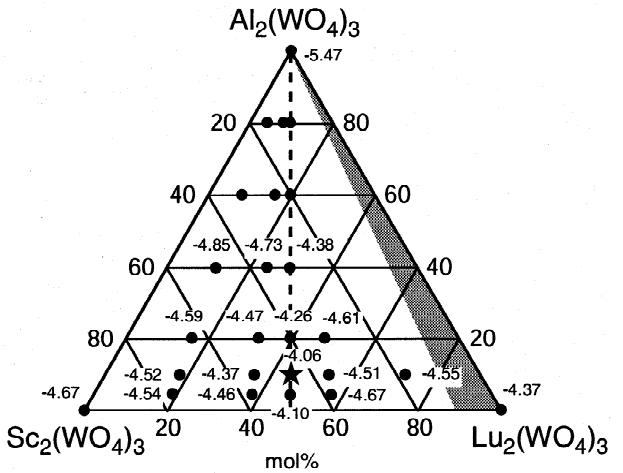

Fig. 8. Relationship between the conductivity at 600°C in the log σ expression and the composition of the $Al_2(WO_4)_3$–$Sc_2(WO_4)_3$–$Lu_2(WO_4)_3$ solid solution system.

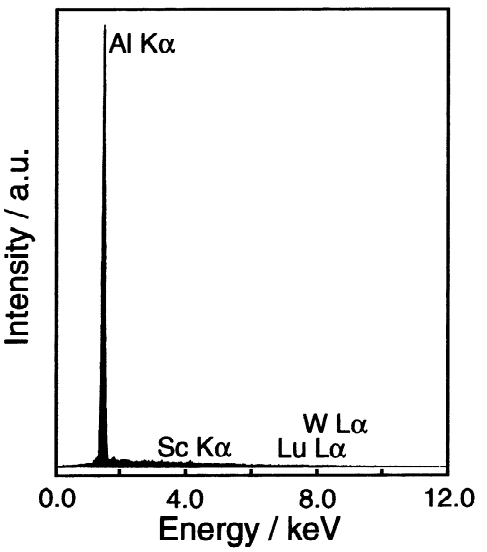

Fig. 9. The EPMA spot analysis of the clusters of ball shape deposits at the cathodic surface of $0.1Al_2(WO_4)_3$–$0.9(Sc_{0.5}Lu_{0.5})_2(WO_4)_3$ after electrolysis.

around zero which declares that the predominant charge carrier in the $(1-x)Sc_2(WO_4)_3$–$xGd_2(WO_4)_3$ system changed from ion ($x<0.6$) to electron or hole ($x>0.6$).

In order to enhance the low Al^{3+} conduction in $Al_2(WO_4)_3$ ($Al_2(WO_4)_3$ shows the lowest conductivity as depicted in Fig. 3), the $Al_2(WO_4)_3$–$Sc_2(WO_4)_3$–$Lu_2(WO_4)_3$ solid solutions were prepared. By mixing three cations with different size, the various lattice size was successfully realized. In the solid solution, it is expected that both Sc^{3+} and Lu^{3+} (0.1001 nm) with larger size compared with Al^{3+} (0.0675 nm) function as the constituent cation of the lattice conformer and the smallest Al^{3+} cation conducts in the expanded lattice.

Fig. 8 presents the conductivities of the various $Al_2(WO_4)_3$–$Sc_2(WO_4)_3$–$Lu_2(WO_4)_3$ solid solutions at 600°C. The $0.1Al_2(WO_4)_3$–$0.9(Sc_{0.5}Lu_{0.5})_2(WO_4)_3$ solid solution (★) exhibited the highest conductivity which is 25 times as high as that of pure $Al_2(WO_4)_3$. After the dc electrolysis of the $0.1Al_2(WO_4)_3$–$0.9(Sc_{0.5}Lu_{0.5})_2(WO_4)_3$ solid solution, a lot of ball shape clusters were recognized at the cathodic surface and the element detected by EPMA is only aluminum in the deposits without any Sc, Lu, and W element as presented in Fig. 9. This result explicitly indicates that the only Al^{3+} migrates in the $0.1Al_2(WO_4)_3$–$0.9(Sc_{0.5}Lu_{0.5})_2(WO_4)_3$ solid solution and Sc^{3+} and Lu^{3+} cations function to be the conformer of the solid solution lattice.

4. Conclusions

The trivalent rare earth ion conduction in tungstates and molybdates with $Sc_2(WO_4)_3$ type structure was directly

demonstrated by the dc electrolysis, and $Sc_2(WO_4)_3$ and $Sc_2(MoO_4)_3$ were found to possess the highest conductivity among each solid electrolyte series, respectively. The $Sc_2(WO_4)_3$ type solid electrolyte shows the trivalent ionic conducting characteristics in a wide O_2 pressure range (P_{O_2}: 10^{-17}–10^5 Pa for tungstate, 10^{-13}–10^5 Pa for molybdate). The most suitable lattice size for the trivalent R^{3+} cation conduction in $R_2(MO_4)_3$ was clarified by preparing the various types of solid solutions. For the Sc^{3+} ion conduction, the optimum lattice was obtained for the $0.8Sc_2(WO_4)_3$–$0.2Gd_2(WO_4)_3$ solid solution and the Sc^{3+} ion conductivity enhanced three times higher than that of pure $Sc_2(WO_4)_3$. The highest Al^{3+} conductivity in $Sc_2(WO_4)_3$ type structure was realized for the $0.1Al_2(WO_4)_3$–$0.9(Sc_{0.5}Lu_{0.5})_2(WO_4)_3$ solid solution and the conductivity was 25 times as high as that of $Al_2(WO_4)_3$. In both solid solution systems, the migrating cation species were directly identified to be the smallest trivalent cation among the constituent trivalent cations in the structure. The larger trivalent cations among in the $Sc_2(WO_4)_3$ type structure functions to expand the solid solution crystal lattice and this results in the smooth ion conduction of the smallest trivalent ion in the structure.

Acknowledgements

The present work was partially supported by a Grant-in-Aid for Scientific Research No. 09215223 on Priority Areas (No. 260), Nos. 06241106, 06241107, and 093065 from The Ministry of Education, Science, Sports and Culture. This work was also supported by the ‘Research for the Future, Preparation and Application of Newly Designed Solid Electrolytes(JSPS-RFTF96P00102)’ Program from the Japan Society for the Promotion of Science.

References

[1] B. Dunn, G.C. Farrington, Solid State Ionics 9 and 10 (1983) 223.
[2] W. Carrillo-Cabrera, J.O. Thomas, G.C. Farrington, Solid State Ionics 9 and 10 (1983) 245.
[3] B. Ghosal, E.A. Mangle, M.R. Tipp, B. Dunn, G.C. Farrington, Solid State Ionics 9 and 10 (1983) 273.
[4] G.C. Farrington, B. Dunn, J.O. Thomas, Appl. Phys. A32 (1983) 159.
[5] T. Dedecke, J. Köhler, F. Tietz, W. Urland, Eur. J. Solid State Inorg. Chem. 33 (1996) 185.
[6] J. Köhler, W. Urland, Solid State Ionics 86–88 (1996) 93.
[7] J. Köhler, W. Urland, Angew. Chem. 109 (1997) 105.
[8] A.M. George, A.N. Virkar, J. Phys. Chem. Solid. 49 (1998) 743.
[9] T.E. Warner, D.J. Fray, A. Davies, Solid State Ionics 92 (1996) 99.
[10] Y. Kobayashi, T. Egawa, S. Tamura, N. Imanaka, G. Adachi, Chem. Mater. 9 (1997) 1649.
[11] N. Imanaka, Y. Kobayashi, G. Adachi, Chem. Lett. (1995) 433.
[12] N. Imanaka, G. Adachi, J. Alloys Comp. 250 (1997) 492.
[13] N. Imanaka, Y. Kobayashi, K. Fujiwara, T. Asano, Y. Okazaki, G. Adachi, Chem. Mater. 10 (1998) 2006.
[14] N. Imanaka, G. Adachi, Molten Solts 41 (1998) 177.
[15] N. Imanaka, Y. Kobayashi, S. Tamura, G. Adachi, Electrochem. Solid-State Lett. 1 (1998) 271.
[16] Y. Kobayashi, S. Tamura, N. Imanaka, G. Adachi, Solid State Ionics 113–115 (1998) 545.
[17] F. Izumi, The Rietveld Method, Oxford University Press, Oxford, 1993, Chapter 13.
[18] Y. Kobayashi, T. Egawa, Y. Okazaki, S. Tamura, N. Imanaka, G. Adachi, Solid State Ionics 111 (1998) 59.
[19] Y. Kobayashi, T. Egawa, S. Tamura, N. Imanaka, G. Adachi, Solid State Ionics 118 (1999) 325.
[20] S. Tamura, T. Egawa, Y. Okazaki, Y. Kobayashi, N. Imanaka, G. Adachi, Chem. Mater. 10 (1998) 1958.
[21] R.D. Shannon, Acta Cryst. A32 (1976) 751.